Lu, X.; Schieda, M.; Blawert, C.; Kainer, K.U.; Zheludkevich, M.L.:

Formation of photocatalytic plasma electrolytic oxidation coatings on magnesium alloy by incorporation of TiO2 particles

In: Surface and Coatings Technology (2016) Elsevier

DOI: 10.1016/j.surfcoat.2016.09.006

Formation of photocatalytic plasma electrolytic oxidation coatings on magnesium alloy by incorporation of TiO_2 particles

Xiaopeng Lu[a]*, Mauricio Schieda[a], Carsten Blawert[a], Karl Ulrich Kainer[a], Mikhail L. Zheludkevich[a,b]

[a]Institute of Materials Research, Helmholtz-Zentrum Geesthacht, Max-Plank-Str. 1, 21502 Geesthacht, Germany

[b]Department of Materials and Ceramic Engineering, CICECO-Aveiro Institute of Materials, University of Aveiro, 3810-193 Aveiro, Portugal

Corresponding author: Phone: +494152871943, Fax: +494152871960,

Email: xiaopeng.lu@hzg.de

Abstract

Photocatalytically active plasma electrolytic oxidation coatings on AM50 Mg alloy are reported in the present work. The photocatalytic activity was achieved via introduction of anatase (TiO_2 particles) to the treatment bath. The photocatalytic performance of the coating was evaluated by measuring the degradation rate of aqueous methylene blue solution and was primarily related to the anatase content on the coating surface. Lower treatment voltage and a higher amount of particles in the electrolyte can be used to incorporate more anatase into the layer and generate superior photocatalytic coatings. The tailored and functionalized surface provides new functionality for magnesium alloys.

Keywords

Magnesium alloy; Plasma electrolytic oxidation; Photocatalytic activity; TiO_2 particles

1. Introduction

Plasma electrolytic oxidation (PEO) is a promising surface treatment process derived from conventional anodizing to form ceramic-like coatings on light metals, which can be used for industrial (corrosion and wear) and biomedical applications [1-5]. However, it is generally claimed that the coatings have high porosity and limited variations in phase composition. Addition of particles to the PEO electrolytes has been explored as a new strategy to provide a wider range of compositions and enhanced properties for PEO coatings [6-10]. Particles can be incorporated either reactively or inertly into the coatings, depending on the size and melting point of the particles as well as the treatment conditions [11]. Titanium dioxide is a well-known photocatalytic material that exists in two main polymorphs, anatase and rutile [12]. Anatase transforms irreversibly to rutile at elevated temperatures, in the range of 400-1200 °C [13, 14]. Generally, anatase TiO_2 exhibits higher photocatalytic activity than rutile TiO_2. The phase mixture of different polymorphs is proved to show synergistic effects and better photocatalytic activity is observed compared with pure phases [15]. Hence, it can be inferred that inertly incorporated TiO_2 particles via PEO technique may enable Mg alloy surface with photocatalytic properties. Consequently, the TiO_2 doped PEO coatings can provide Mg-based biodegradable implants with bioactivity and antibacterial properties. Such coatings can also offer enhanced UV sterilization ability for Mg alloys used in consumer electronics or automotive interiors. Although there are studies about photocatalytic performance of PEO coatings [16-18], the influence of TiO_2 particles on the photocatalytic properties of PEO coated Mg alloy is not yet fully understood. It has been proved that the particle content in the coating increases with the particle concentration in the electrolyte [19, 20]. The applied electrical parameters also have a huge

effect on the incorporation mode of particles, since electrophoretic force is one of the main driving forces to attract particles to the layer [21, 22]. In this study, the effect of TiO_2 particle concentration and the applied voltage on the morphology, composition and photocatalytic performance of the PEO coatings are investigated. The role of the incorporated particles and electrical parameters applied during PEO treatment in the photocatalytic activity of PEO coatings on AM50 Mg alloy is revealed.

2. Experimental

Specimens of AM50 Mg alloy with a size of 15 mm × 15 mm × 4 mm were prepared from gravity cast ingot material. The chemical composition of the alloy in wt.%, as measured with an Arc Spark OES (Spark analyser M9, Spectro Ametek, Germany), is 4.74% Al, 0.383% Mn, 0.065% Zn, 0.063% Si, 0.002% Fe, 0.002% Cu and Mg balance. The specimens were ground using emery papers up to 1200 grit and then air-dried prior to PEO treatment. The PEO process was performed by using a pulsed DC power source with a pulse ratio of t_{on}: t_{off} = 0.4 ms: 3.6 ms. The specimen and a stainless steel tube were used as the anode and cathode, respectively. Different amounts of anatase particles (5 g/L, 10 g/L and 20 g/L) were added to hexametaphosphate based electrolyte (5 g/L KOH and 20 g/L $Na_6P_6O_{18}$). The morphology and XRD pattern of the anatase powder (average particle size of 200 nm) is shown Fig. 1. Reference coatings were also produced from electrolyte free of particles. Constant voltage of 400 V and 500 V for 10 min was used for the PEO treatments and the maximum average current density was limited to 300 mA/cm^2. The corresponding coatings are named as PPEO (no-400V), PPEO (no-500V), PPEO (5g-400V), PPEO (5g-500V), PPEO (10g-400V), PPEO (10g-500V), PPEO (20g-400V), and PPEO (20g-500V), respectively. A scanning electron microscope (TESCAN Vega3 SB) combined with an energy dispersive spectrometer (EDS) system from eumeX

(XRFSystems) was used to examine the surface morphology and composition of the coatings. The phase composition of the coatings was measured by a Bruker X-ray diffractometer using Cu Kα radiation.

The photocatalytic activity of the PEO coatings was evaluated by measuring the degradation rate of aqueous methylene blue (MB) solution. The solution was exposed to light emitted from an incandescent light bulb (OSRAM ULTRA-VITALUX 300 W) for 8 h. The concentration of the MB solution was 5.6 mg/L and the solution volume was 20 ml. An UV-Vis spectrophotometer (Shimadzu UV-1240) was used to measure the concentration change of the MB solution, based on the Beer–Lambert equation stating $A = \varepsilon \times l \times C$ where A, ε, l, and C are absorption of the solution, molar absorptivity, path length, and solution concentration, respectively. Since l and ε are constant, the parameter C is linearly proportional to the absorption. The evolution of absorption of MB solution at $\lambda = 663$ nm was measured every 2 h.

3. Results and Discussion

3.1. Microstructure

The surface morphology of the PEO coatings is shown in Fig. 2. The coating surface is dominated by pores and is not significantly influenced either by the additional particles in the electrolyte or by the applied voltage during PEO treatment, except for the coatings with addition of 20 g/L particles (Fig. 2g and h) which reveal a lower number and smaller size of pores. Fig. 3 shows the cross sections of the different coatings. It is apparent that the thickness of the coating has been reduced significantly when utilizing particle-containing electrolytes. A higher amount of particles in the electrolyte is evidently detrimental to the coating growth. However, the

coatings become thicker at the same amount of particles with the increase of applied voltage from 400 V to 500 V.

3.2. Coating composition

EDS analysis (Fig. 4) of the coating surface was performed to investigate the uptake of the particles into the layer. The Ti content increases significantly with the particle concentration in the electrolyte and applied voltage during PEO treatment. For instance, the Ti content in coating with 5 g/L particle addition increases from approximately 2.5 at. % to 5.2 at. % with the increase of applied voltage. The particle amount in PPEO (20g-400V) is seven times higher than PPEO (5g-400V). The X-ray diffraction patterns of the coatings are depicted in Fig. 5. It can be seen that all the coatings are composed of amorphous phase in the 2θ range of 20-35°, possibly containing phosphorus. The appearance of Mg peaks in all conditions is due to the penetration of the X-ray through the whole layer and reaching the substrate. Anatase peaks are visible for all the particle-containing coatings, indicating that the particles are inertly incorporated into the PEO layer. MgO peak only occurs in the layers with addition of 10 and 20 g/L particles, suggesting that the trapped particles might act as nucleation sites for crystallization of the coating. It is worthwhile to note that some of the original anatase was transformed to rutile when applying higher voltage and increasing the particle concentration. In particular, small amount of reactive phase (Mg_2TiO_4) was detected for coatings with 20 g/L particle addition under 500 V, suggesting that different incorporation modes (inert and partly reactive incorporation) can be achieved for anatase under various treatment parameters.

3.3. Photocatalytic activity

The photocatalytic activity of the PEO coatings is shown in Fig. 6. The concentration of the methylene blue decreases slightly without huge difference for all the coatings after 2 h immersion. Afterwards, the degradation rate of MB solution speeds up, especially for the coatings with higher content of particles. It was found that the coatings synthesized under 400 V with addition of 20 g/L particles demonstrated the optimum photoactivity. Although higher voltage leads to incorporation of more particles into the coating, it is detrimental to the photocatalytic activity of the coatings. This is probably due to the transformation of anatase to rutile and/or Mg_2TiO_4. Moreover, particles that are enriched on the coating surface are more effective to the photocatalytic performance compared with the particles existing in the internal layer, since the Ti content of PPEO (20g-400V) is much higher than that of the other coatings (Fig. 7). Therefore, the amount of the inertly incorporated anatase close to the surface plays a dominant role in the photocatalytic properties of PEO coatings on Mg alloy. Additionally, the photocatalytic activity (Fig. 8) of PPEO (20g-400V) is even superior to PEO coating formed directly on Ti alloy using parameters according to [23]. It has been reported that the photocatalytic property of TiO_2 decreases with an increase of the particles size [24]. It can be inferred that addition of TiO_2 nanoparticles is more effective in improving the photocatalytic performance of the layer in comparison to the bulk material (TiO_2) in PEO coated Ti alloy.

4. Conclusions

Introduction of anatase (TiO_2 particles) into PEO coatings enables new photocatalytic functionality for Mg and its alloy. Anatase was partially transformed to rutile as well as small amount of Mg_2TiO_4, which can be controlled by the treatment parameters. The photocatalytic performance of the coating is primarily related to the anatase content on the coating surface. Lower treatment voltage and a higher amount of particles in the electrolyte can be used to

generate superior photocatalytic PEO coatings. Such coatings may offer improved UV sterilization ability to degradable Mg implants or potential anti-bacterial properties for Mg alloys used in consumer electronics or automotive interiors.

Acknowledgements

The technical support of Mr. Volker Heitmann and Mr. Ulrich Burmester during this work is gratefully acknowledged. X. Lu thanks China Scholarship Council (201207090010) for the award of fellowship and funding.

References

[1] A.L. Yerokhin, X. Nie, A. Leyland, A. Matthews, S.J. Dowey, Plasma electrolysis for surface engineering, Surface and Coatings Technology, 122 (1999) 73-93.
[2] J.A. Curran, T.W. Clyne, The thermal conductivity of plasma electrolytic oxide coatings on aluminium and magnesium, Surface and Coatings Technology, 199 (2005) 177-183.
[3] M.P. Staiger, A.M. Pietak, J. Huadmai, G. Dias, Magnesium and its alloys as orthopedic biomaterials: A review, Biomaterials, 27 (2006) 1728-1734.
[4] R. Arrabal, E. Matykina, T. Hashimoto, P. Skeldon, G.E. Thompson, Characterization of AC PEO coatings on magnesium alloys, Surface and Coatings Technology, 203 (2009) 2207-2220.
[5] G. Wu, J.M. Ibrahim, P.K. Chu, Surface design of biodegradable magnesium alloys — A review, Surface and Coatings Technology, 233 (2013) 2-12.
[6] T.S. Lim, H.S. Ryu, S.-H. Hong, Electrochemical corrosion properties of CeO2-containing coatings on AZ31 magnesium alloys prepared by plasma electrolytic oxidation, Corrosion Science, 62 (2012) 104-111.
[7] K.M. Lee, B.U. Lee, S.I. Yoon, E.S. Lee, B. Yoo, D.H. Shin, Evaluation of plasma temperature during plasma oxidation processing of AZ91 Mg alloy through analysis of the melting behavior of incorporated particles, Electrochimica Acta, 67 (2012) 6-11.
[8] M. Mohedano, C. Blawert, M.L. Zheludkevich, Silicate-based Plasma Electrolytic Oxidation (PEO) coatings with incorporated CeO2 particles on AM50 magnesium alloy, Materials & Design, 86 (2015) 735-744.
[9] R. Arrabal, M. Mohedano, E. Matykina, A. Pardo, B. Mingo, M.C. Merino, Characterization and wear behaviour of PEO coatings on 6082-T6 aluminium alloy with incorporated α-Al2O3 particles, Surface and Coatings Technology, 269 (2015) 64-73.
[10] S. Stojadinović, N. Tadić, N. Radić, B. Stojadinović, B. Grbić, R. Vasilić, Synthesis and characterization of Al2O3/ZnO coatings formed by plasma electrolytic oxidation, Surface and Coatings Technology, 276 (2015) 573-579.
[11] X. Lu, C. Blawert, Y. Huang, H. Ovri, M.L. Zheludkevich, K.U. Kainer, Plasma electrolytic oxidation coatings on Mg alloy with addition of SiO2 particles, Electrochimica Acta, 187 (2016) 20-33.
[12] D.H. Hanaor, C. Sorrell, Review of the anatase to rutile phase transformation, J Mater Sci, 46 (2011) 855-874.

[13] P.I. Gouma, M.J. Mills, Anatase-to-rutile transformation in titania powders, J Am Ceram Soc, 84 (2001) 619-622.
[14] J. Kim, K.C. Song, S. Foncillas, S.E. Pratsinis, Dopants for synthesis of stable bimodally porous titania, J Eur Ceram Soc, 21 (2001) 2863-2872.
[15] D.O. Scanlon, C.W. Dunnill, J. Buckeridge, S.A. Shevlin, A.J. Logsdail, S.M. Woodley, C.R.A. Catlow, M.J. Powell, R.G. Palgrave, I.P. Parkin, G.W. Watson, T.W. Keal, P. Sherwood, A. Walsh, A.A. Sokol, Band alignment of rutile and anatase TiO2, Nat Mater, 12 (2013) 798-801.
[16] Y.-K. Shin, W.-S. Chae, Y.-W. Song, Y.-M. Sung, Formation of titania photocatalyst films by microarc oxidation of Ti and Ti–6Al–4V alloys, Electrochemistry Communications, 8 (2006) 465-470.
[17] X. Jiang, Y. Wang, C. Pan, Micro-arc oxidation of TC4 substrates to fabricate TiO2/YAG:Ce3+ compound films with enhanced photocatalytic activity, Journal of Alloys and Compounds, 509 (2011) L137-L141.
[18] W. Li, M. Tang, L. Zhu, H. Liu, Formation of microarc oxidation coatings on magnesium alloy with photocatalytic performance, Applied Surface Science, 258 (2012) 10017-10021.
[19] M. Tang, W. Li, H. Liu, L. Zhu, Influence of titania sol in the electrolyte on characteristics of the microarc oxidation coating formed on 2A70 aluminum alloy, Surface and Coatings Technology, 205 (2011) 4135-4140.
[20] X. Lu, C. Blawert, M.L. Zheludkevich, K.U. Kainer, Insights into plasma electrolytic oxidation treatment with particle addition, Corrosion Science, 101 (2015) 201-207.
[21] D.-Y. Kim, M. Kim, H.-E. Kim, Y.-H. Koh, H.-W. Kim, J.-H. Jang, Formation of hydroxyapatite within porous TiO2 layer by micro-arc oxidation coupled with electrophoretic deposition, Acta Biomaterialia, 5 (2009) 2196-2205.
[22] K.M. Lee, K.R. Shin, S. Namgung, B. Yoo, D.H. Shin, Electrochemical response of ZrO2-incorporated oxide layer on AZ91 Mg alloy processed by plasma electrolytic oxidation, Surface and Coatings Technology, 205 (2011) 3779-3784.
[23] R. Kumari, C. Blawert, J.D. Majumdar, Microstructures and Properties of Plasma Electrolytic Oxidized Ti Alloy (Ti-6Al-4V) for Bio-implant Application, Metallurgical and Materials Transactions A, 47 (2015) 788-800.
[24] H. Lin, C.P. Huang, W. Li, C. Ni, S.I. Shah, Y.-H. Tseng, Size dependency of nanocrystalline TiO2 on its optical property and photocatalytic reactivity exemplified by 2-chlorophenol, Applied Catalysis B: Environmental, 68 (2006) 1-11.

Fig. 1 Morphology and XRD pattern of the anatase powder.

Fig. 2 Surface morphology of different coatings (a) PPEO (no-400V), (b) PPEO (no-500V), (c) PPEO (5g-400V), (d) PPEO (5g-500V), (e) PPEO (10g-400V), (f) PPEO (10g-500V), (g) PPEO (20g-400V) and (h) PPEO (20g-500V).

Fig. 3 Cross section of different coatings (a) PPEO (no-400V), (b) PPEO (no-500V), (c) PPEO (5g-400V), (d) PPEO (5g-500V), (e) PPEO (10g-400V), (f) PPEO (10g-500V), (g) PPEO (20g-400V) and (h) PPEO (20g-500V).

Fig. 4 Ti content on the surface of the coatings (1) PPEO (no-400V), (2) PPEO (no-500V), (3) PPEO (5g-400V), (4) PPEO (5g-500V), (5) PPEO (10g-400V), (6) PPEO (10g-500V), (7) PPEO (20g-400V) and (8) PPEO (20g-500V).

Fig. 5 XRD patterns of the different coatings (a) coatings produced under 400V, (b) coatings produced under 500V.

Fig. 6 Photocatalytic activity of the PEO coatings.

Fig. 7 Mapping (a) PPEO (20g-400V); Line scan (b) PPEO (20g-400V), (c) PPEO (10g-400V) and (d) PPEO (20g-500V).

Fig. 8 Comparison of the photocatalytic activity of PEO coatings on Mg alloy and Ti alloy.

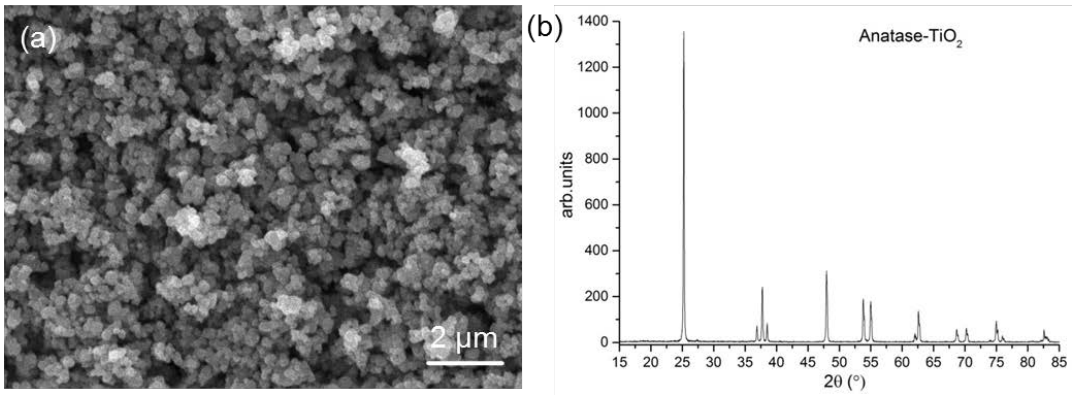

Fig. 1

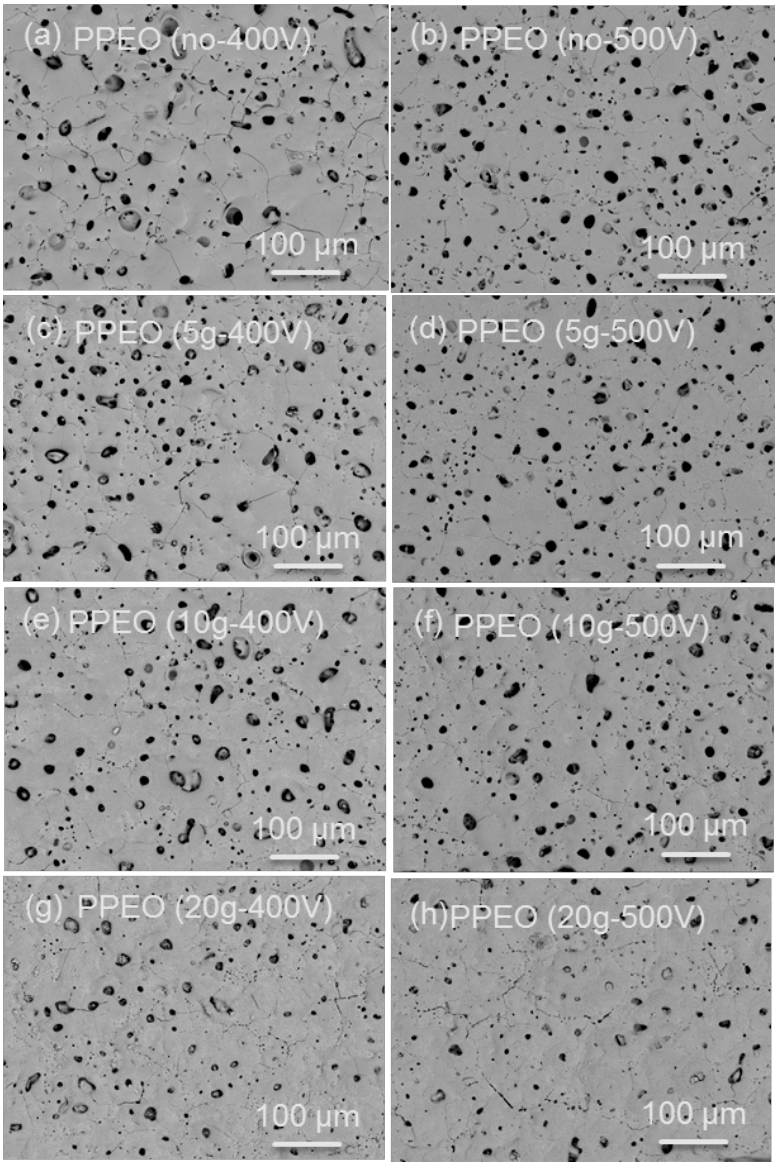
(a) PPEO (no-400V)
100 μm
(b) PPEO (no-500V)
100 μm
(c) PPEO (5g-400V)
100 μm
(d) PPEO (5g-500V)
100 μm
(e) PPEO (10g-400V)
100 μm
(f) PPEO (10g-500V)
100 μm
(g) PPEO (20g-400V)
100 μm
(h)PPEO (20g-500V)
100 μm

Fig. 2

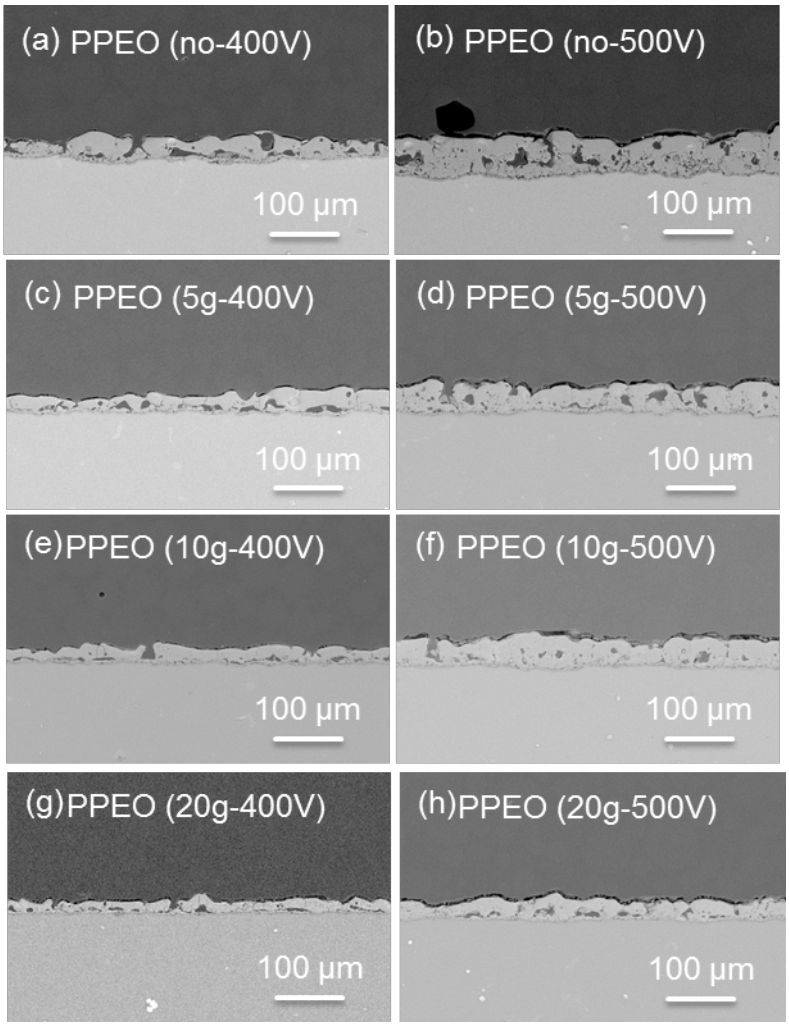
(a) PPEO (no-400V)
100 μm
(b) PPEO (no-500V)
100 μm
(c) PPEO (5g-400V)
100 μm
(d) PPEO (5g-500V)
100 μm
(e)PPEO (10g-400V)
100 μm
(f) PPEO (10g-500V)
100 μm
(g)PPEO (20g-400V)
100 μm
(h)PPEO (20g-500V)
100 μm

Fig. 3

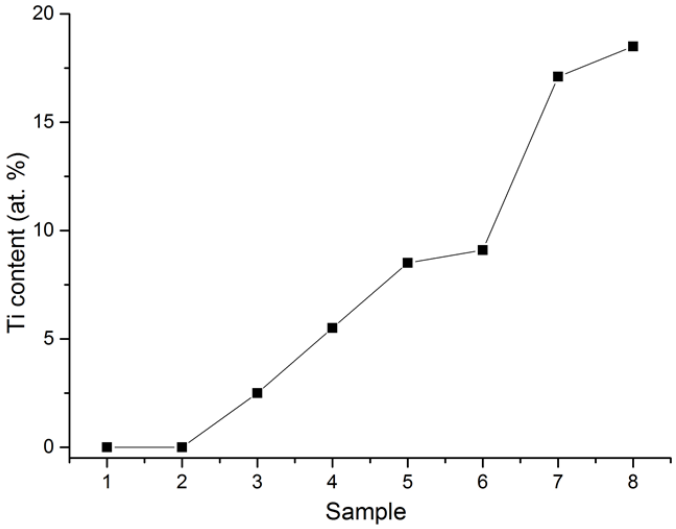
Ti content (at. %)
Sample
0
5
10
15
20
1
2
3
4
5
6
7
8

Fig. 4

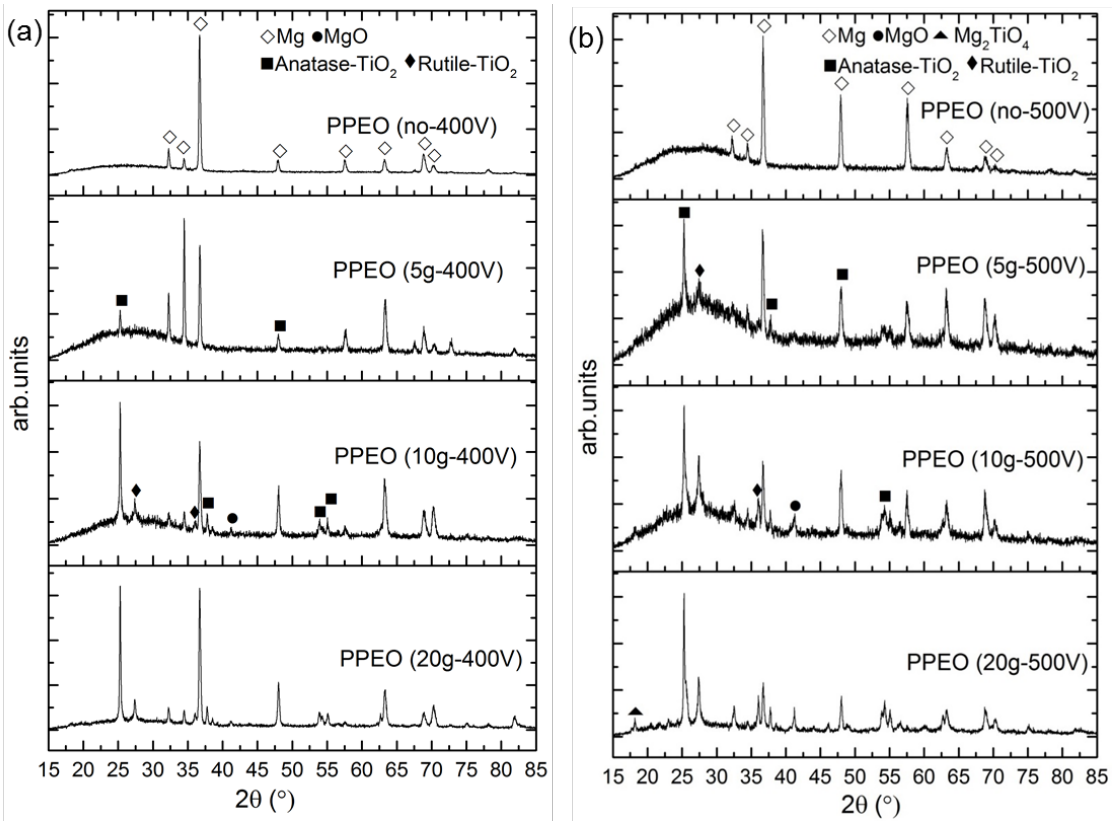
(a)
◇Mg ●MgO
■Anatase-TiO2 ♦Rutile-TiO2
PPEO (no-400V)
PPEO (5g-400V)
PPEO (10g-400V)
PPEO (20g-400V)
arb.units
15 20 25 30 35 40 45 50 55 60 65 70 75 80 85
2θ (°)
(b)
◇Mg ●MgO ▲Mg2TiO4
■Anatase-TiO2 ♦Rutile-TiO2
PPEO (no-500V)
PPEO (5g-500V)
PPEO (10g-500V)
PPEO (20g-500V)
arb.units
15 20 25 30 35 40 45 50 55 60 65 70 75 80 85
2θ (°)

Fig. 5

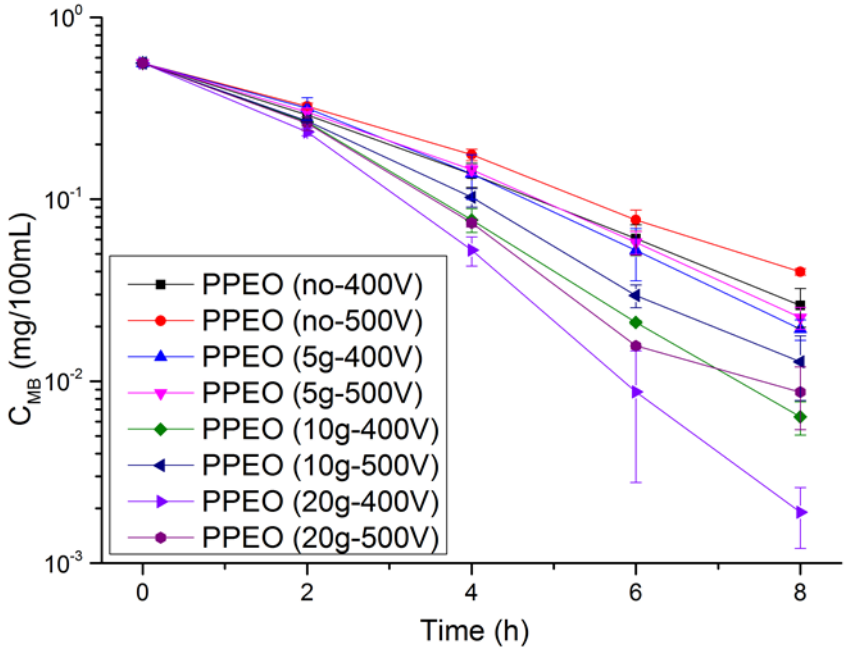
10^0
10^{-1}
10^{-2}
10^{-3}
C_{MB} (mg/100mL)
0
2
4
6
8
Time (h)
PPEO (no-400V)
PPEO (no-500V)
PPEO (5g-400V)
PPEO (5g-500V)
PPEO (10g-400V)
PPEO (10g-500V)
PPEO (20g-400V)
PPEO (20g-500V)

Fig. 6

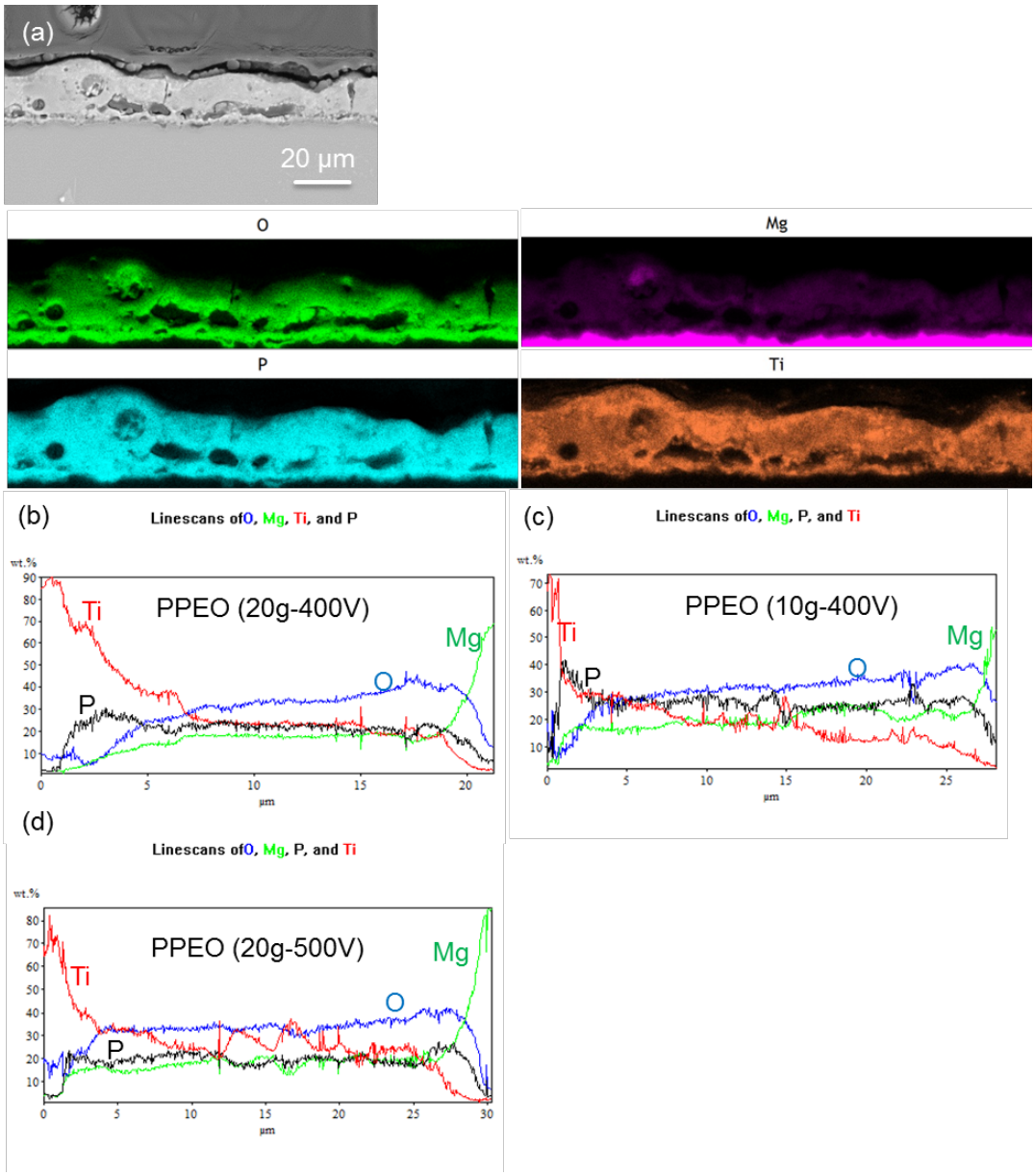
(a)
20 µm
O
Mg
P
Ti
(b)
Linescans ofO, Mg, Ti, and P
wt.%
PPEO (20g-400V)
Ti
Mg
O
P
µm
(c)
Linescans ofO, Mg, P, and Ti
wt.%
PPEO (10g-400V)
Ti
Mg
O
P
µm
(d)
Linescans ofO, Mg, P, and Ti
wt.%
PPEO (20g-500V)
Ti
Mg
O
P
µm

Fig. 7

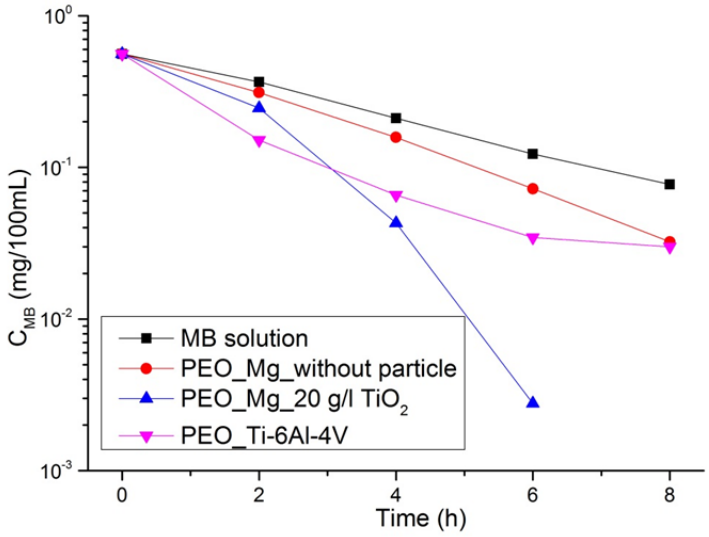
10^0
10^{-1}
10^{-2}
10^{-3}
C_{MB} (mg/100mL)
0
2
4
6
8
Time (h)
MB solution
PEO_Mg_without particle
PEO_Mg_20 g/l TiO_2
PEO_Ti-6Al-4V

Fig. 8